Towards a set-based detector for GNSS integrity monitoring

1st Jingyao Su
Institut für Erdmessung
Leibniz Universität Hannover
Hannover, Germany
suj@ife.uni-hannover.de

2nd Steffen Schön
Institut für Erdmessung
Leibniz Universität Hannover
Hannover, Germany
schoen@ife.uni-hannover.de

3rd Mathieu Joerger
Dept. of Aerospace and Ocean Engineering
Virginia Tech
Blacksburg, VA, US
joerger@vt.edu

***Abstract*—This paper aims to evaluate the performance of the set-based fault detection. This approach differs from probabilistic residual-based (RB) or solution separation (SS) fault detection and exclusion methods utilized in the Receiver Autonomous Integrity Monitoring (RAIM) and Advanced RAIM. In the basic positioning model, measurement-level intervals are constructed based on the investigated error models and propagated in a linear manner using interval mathematics and set theory. Convex polytope solutions provide a measure of observation consistency formulated as a constraint satisfaction problem. Consistency checks performed using set operations facilitate multiple-fault detection. Choosing set-emptiness as the detection criterion can alleviate the need for multiple test statistics. In this paper, we formulate the fault detection problem in the context of measurement intervals and propose a framework of integrity monitoring for the set-based detection. Considering a probabilistic error model, we implement the set-based detection methods and assess its integrity performance using Monte Carlo simulations. These evaluations will serve as a basis for further development of efficient estimators and integrity monitors.**

***Index Terms*—GNSS integrity, error modeling, fault detection, set theory, interval mathematics**

I. Introduction

GNSS integrity monitoring methods, including Receiver Autonomous Integrity Monitoring (RAIM) and Advanced RAIM (ARAIM) are using residual-based (RB) approaches or solution separation (SS) for fault detection and exclusion. While being widely implemented in aviation [1]–[3], integrity concepts have not yet achieved a similar level of maturity for land navigation. To fill this gap, detectors and estimators utilizing different strategies have been investigated in recent years, e.g., [4], [5].

Measurement error modeling is foundational to integrity evaluation methods. Overbounding theory can account for stochastic error sources in GNSS [6], [7]. However, error distributions for rarely-occurring, rarely-observed undetected faults are unknown, and error calibration for user receiver and antenna biases is not scalable across equipment manufacturers and models. Thus, systematic uncertainty remains that can dominate the error budget. To bound those systematic errors, interval mathematics and set theory have been investigated in prior works [8]–[11].

Representing errors as intervals, set-theoretic methods explore the linear uncertainty propagation in localization problems, computing confidence zones in which the user is claimed to be located with a given confidence or risk [12]–[14]. For linear estimators, measurement-level intervals have an impact on estimation states that can be expressed as a set of inequalities. For example, a least-squares estimator produces predictive error bounds represented by zonotopes, [15], [16].

In the presence of sample measurement errors, interval solutions provide a measure of observation inconsistency formulated as a constraint satisfaction problem in [17]. Geometrical constraints formed by interval bounds result in a polytopic solution set: this inconsistency area serves as a basis for fault detection through set operations [18]. Applications can be seen across various domains, e.g., robot localization [19], autonomous boats [20], Instrument Landing System [21]. In set-based detection, set-emptiness is used as a detection criterion which alleviates the need for multiple test statistics in the framework of multiple hypothesis testing. However, there is currently no process to evaluate the false alert probability, which then depends on measurement uncertainty intervals. Studies like [14], [22], [23] investigated only the risk based on Gaussian distributed error model without considering unknown distributed faults. The potential of set-based approaches to tighten integrity and continuity risk bounds has yet to be explored.

The main contributions of this paper are twofold:

- We formulate the fault detection problem for GNSS integrity monitoring in the context of measurement intervals and show a relationship between detection intervals, error distributions, and feasible set solutions;
- Through a benchmark example, we implement and evaluate the probability of loss of continuity and loss of integrity for the set-based detector. The performance of the set-based detection is compared with classical RB/SS detectors in terms of critical integrity events by Monte Carlo simulations. We show that the continuity risk of set-based detector can be effectively assessed, and the feasible set solution from measurement interval constraints assures high integrity for all elements. We

This work was supported by the German Research Foundation as part of the Research Training Group 2159: Integrity and Collaboration in Dynamic Sensor Networks (i.c.sens).

978-1-6654-1772-3/23/$31.00 ©2023 IEEE

demonstrate the need of designing optimal set estimation to tighten the integrity risk bound. These will serve as a basis to further development in the set-based integrity monitoring approach.

The remainder of the paper is organized as follows: Sec. II briefly introduces the basics of interval and set representations. Sec. III describes the paper's fundamental assumptions, in particular, the fault detection in context of measurement error intervals. Sec. IV reviews the concepts of continuity and integrity in conventional RAIM/ARAIM approaches, i.e., the residual-based and solution-separation detectors, and then interprets and formulates loss of continuity and loss of integrity for the set-based detector. Sec. V discusses and implements an evaluation strategy through a canonical example to demonstrate the procedures and performance of the set-based detection.

II. Basics of interval and set representation

Intervals are represented with their lower bounds and upper bounds in this paper, such as: $[y] = [\underline{y}, \overline{y}]$. The width of an interval is defined as $W([y]) = \overline{y} - \underline{y}$, and its radius is half of the width $rad([y]) = \frac{1}{2}W([y])$. Readers of interest can refer to textbooks, e.g., [12], [24] for more introduction to interval mathematics.

Polytopes can be defined in two ways: the *H-Polytope* and the *V-Polytope*, [25]. The *H-Polytope* used in this paper, denotes an intersection of closed halfspaces, i.e. a set $\mathcal{P} \subseteq \mathbb{R}^m$ presented in the form:

$$\mathcal{P}(\mathbf{H}, \mathbf{b}) = \{\mathbf{z} \in \mathbb{R}^m \mid \mathbf{Hz} \leq \mathbf{b}, \mathbf{H} \in \mathbb{R}^{2n \times m}, \mathbf{b} \in \mathbb{R}^{2n}\} \quad (1)$$

which can be interpreted as the solution set of a finite number of linear inequalities.

Zonotopes form a special class of polytopes: Each zonotope is a convex polytope that is centrally symmetric, [25]. In this paper, we construct the zonotope as the intersection of n pairs of parallel hyperplanes, i.e., [26]

$$\mathcal{Z}(\mathbf{H}, \mathbf{b}) = \{\mathbf{z} \in \mathbb{R}^m | \mathbf{H}(\mathbf{z} - \mathbf{c}_\mathcal{Z}) \leq \mathbf{b}, \mathbf{H} \in \mathbb{R}^{2n \times m}, \mathbf{b} \in \mathbb{R}^{2n}, \mathbf{c}_\mathcal{Z} \in \mathbb{R}^m\} \quad (2)$$

with $\mathbf{c}_\mathcal{Z}$ denoting its center.

III. Fault detection in the context of measurement intervals

A. Observation model and its linearization

The basic satellite positioning problem is usually handled by a first order linearization of the GNSS pseudorange measurement p_r^k between satellite k and receiver r w.r.t approximate values for the states $\mathbf{x}_0$:

$$p_r^k \cong p_{r,0}^k + \mathbf{A}^k \mathbf{x} \quad (3)$$

where $p_{r,0}^k$ is the observation computed using the approximate parameter values and correction models and $\mathbf{A}^k$ the corresponding line of the design matrix (Jacobian), $\mathbf{x}$ the vector of state increments w.r.t to their approximate values $\mathbf{x}_0$, i.e. the total state reads $\mathbf{x}' = \mathbf{x}_0 + \mathbf{x}$. The pre-fit residual observations or observed-minus-computed (OMC) values are computed

$$y^k := p_r^k - p_{r,0}^k \quad (4)$$

and finally for all n observations of one epoch, we get the linear model:

$$\mathbf{y} = \mathbf{Ax} + \mathbf{e} \quad (5)$$

where,

- $\mathbf{y}$: $[n \times 1]$, vector of OMC values
- $\mathbf{A}$: $[n \times m]$, design matrix, indicating the line-of-sights (LOS)
- $\mathbf{x}$: $[m \times 1]$, state vector, representing the offsets of the receiver's position to its approximate values $\mathbf{x}_0$, in addition to the receiver's clock offset
- $\mathbf{e}$: $[n \times 1]$, error vector, containing all the remaining error components.

B. Construction of an interval-based detector

In order to construct a detector, we fix a threshold $\pm\mathbf{d}$ or interval $[\mathbf{d}] = [-\mathbf{d}, \mathbf{d}]$ for the acceptable amount of observation errors. Then, based on Eq. 5, the detector is formulated as the constraint satisfaction problem:

$$\begin{aligned} \mathbf{Ax} &\in \mathbf{y} - \mathbf{e} + [\mathbf{d}] \\ \Leftarrow \mathbf{y} - \mathbf{e} - \mathbf{d} &\leq \mathbf{Ax} \leq \mathbf{y} - \mathbf{e} + \mathbf{d} \end{aligned} \quad (6)$$

With $\mathbf{B} = \begin{bmatrix} \mathbf{A} \\ -\mathbf{A} \end{bmatrix}$ and $\mathbf{b} = \begin{bmatrix} \mathbf{y} - \mathbf{e} + \mathbf{d} \\ -\mathbf{y} + \mathbf{e} + \mathbf{d} \end{bmatrix}$, we obtain a concise version:

$$\mathbf{Bx} \leq \mathbf{b} \quad (7)$$

which results in a feasible set solution:

$$\mathcal{P}(\mathbf{B}, \mathbf{b}) = \{\mathbf{x} \in \mathbb{R}^m | \mathbf{Bx} \leq \mathbf{b}, \mathbf{B} \in \mathbb{R}^{2n \times m}, \mathbf{b} \in \mathbb{R}^{2n}\} \quad (8)$$

This solution is a polytope [25]. Geometrically, each interval constitutes a "slab" ($\mathcal{S}_j$), perpendicular to the j-th LOS, indicating a finite range of the state uncertainty along its direction:

$$\mathcal{S}_j = \left\{\mathbf{dx} \in \mathbb{R}^m \mid \mathbf{A}^j \mathbf{x} \in [y_j - e_j - d_j, y_j - e_j + d_j]\right\} \quad (9)$$

and the polytopic set solution is the intersection of all "slabs".

Considering an ideal error-free situation, i.e., $\mathbf{e} = \mathbf{0}$ in Eq. 5, we obtain:

$$\mathbf{y}^* = \mathbf{A}\, \mathbf{dx}^* \quad (10)$$

where $\mathbf{y}^*$ is interpreted as the OMC vector obtained when all measurement-domain error perfectly corrected and $\mathbf{x}^*$ the compatible, true state vector. Subsequently, the state-domain set solution is expressed as

$$\begin{aligned} \mathcal{Z} &= \{\mathbf{x} \in \mathbb{R}^m \mid \mathbf{Ax} \leq \mathbf{y}^* + \mathbf{d}, -\mathbf{Ax} \leq -\mathbf{y}^* + \mathbf{d}\} \\ &= \{\mathbf{x} \in \mathbb{R}^m \mid \mathbf{A}(\mathbf{x} - \mathbf{x}^*) \leq \mathbf{d}, -\mathbf{A}(\mathbf{x} - \mathbf{x}^*) \leq \mathbf{d}\} \end{aligned} \quad (11)$$

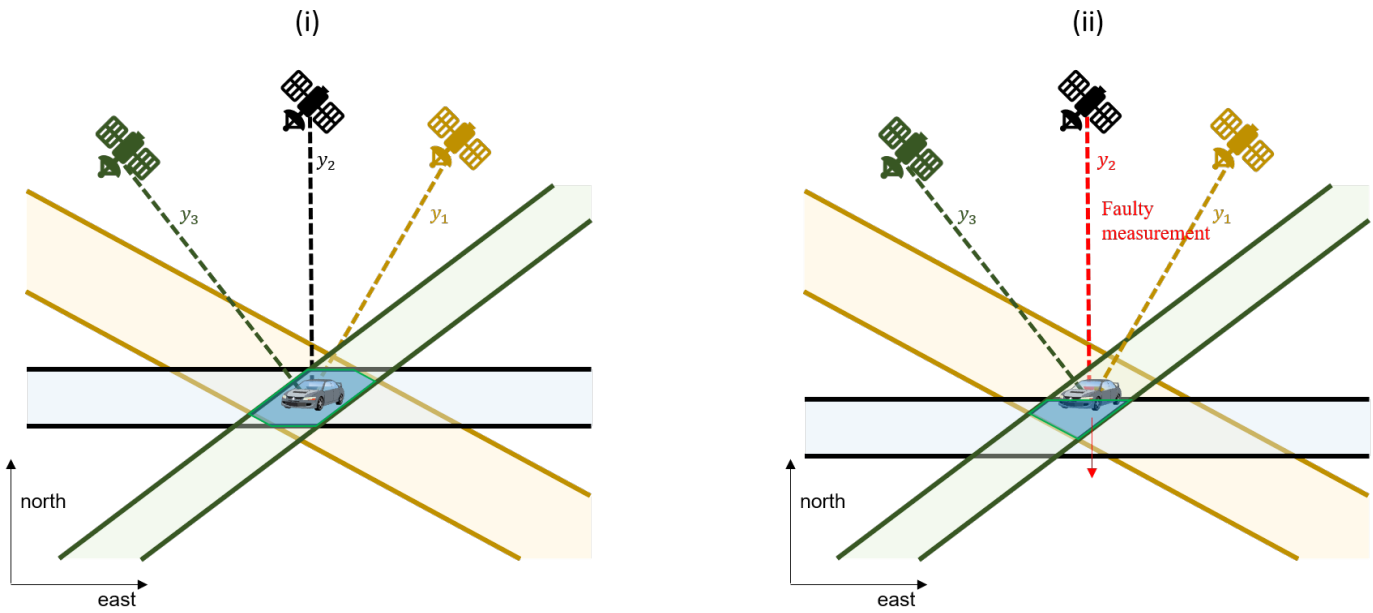

Fig. 1. Conceptual sketch of the two-dimensional slabs and their intersected polytope, with (i) In an ideal noise-free and bias-free case, the intersection is a zonotope. (ii) The intersection of slabs is deformed and shifted in presence of bias in the red line-of-sight.

which is centered at the true state $\mathbf{x}^*$. By definition, it is a zonotope. Fig. 1 (i) illustrates a conceptual sketch of the slabs in the 2D positioning context.

The fault cases are modeled with an additional fault term $\mathbf{f}$. For example, in a specific fault mode H_i, the j-th measurement is biased by the fault magnitude f:

$$\mathbf{A}\mathbf{x} + \mathbf{f} \in \mathbf{y} - \mathbf{e} + [\mathbf{d}],\ \mathbf{f} = [0, ..., f, ..., 0]^T \tag{12}$$

Subsequently, Eq. 7 becomes

$$\mathbf{B}\mathbf{x} + \begin{bmatrix} \mathbf{f} \\ -\mathbf{f} \end{bmatrix} \leq \mathbf{b} \tag{13}$$

Therefore, the feasible set solution $\mathcal{P}$ is deformed and shifted from the fault-free set solution. The deviating direction and magnitude are dependent on both geometry and fault magnitude. For example, the state-domain "slab" associated with the faulty measurement is expressed as:

$$\mathcal{S}_j = \{\mathbf{x} \in \mathbb{R}^m \mid \mathbf{A}^j\mathbf{x} \subseteq [y_j - e_j - d - f, \\ y_j - e_j + d - f]\} \tag{14}$$

In Fig. 1 (ii), the red LOS l_2 is biased to the indicated direction. Once the fault magnitude f excesses a certain value, the feasible solution set becomes an empty set:

$$\mathcal{P} = \emptyset \tag{15}$$

i.e., there is no feasible point solution for the inequalities in Eq. 13, thereby establishing a detection. Graphically, the "slabs" do not intersect.

In order to fulfill requirements of integrity monitoring purposes, it is mandatory to understand the characteristics of this detector under the investigated error models which will be investigated in the next sections.

IV. Loss of Continuity and Loss of Integrity Concepts

A. Conventional RAIM/ARAIM detectors

1) Loss of continuity: The International Civil Aviation Organization (ICAO) defines the continuity of a service as the capability of the system to perform its function without unscheduled interruptions during the intended operation [27]. Therefore, the continuity risk, or probability of loss of continuity (LOC), is the probability of a detected but unscheduled navigation function interruption after an operation has been initiated [28] for aviation applications, expressed as:

$$P_{LOC} = P_{FA} + P_{D,F} + P_{Other} \tag{16}$$

indicating three components:

- P_{FA}: false alert (FA) probability
- $P_{D,F}$: the probability of fault detection when a fault occurs
- P_{Other}: contains other causes of loss of continuity

The first term, the false alert probability is in practice limited by an allocated continuity risk requirement:

$$P_{FA} \leq C_{REQ,0} \tag{17}$$

The other two terms are typically evaluated dependent on dedicated fault models, which is beyond the scope of this work.

Classical RB and SS detectors are designed as comparing individual test statistic q with detection thresholds T that are derived from Eq. 17. For example, under the fault-free hypothesis H_0, the RB threshold T_{RB} is defined as:

$$P\left(|q_{RB}| \geq T_{RB} \mid H_0\right) P(H_0) \leq C_{REQ,0} \tag{18}$$

where q_{RB} is the RB test statistic. SS detection (normalized) thresholds $T_{SS,i}$, w.r.t each fault mode $i, i \in \{1, ..., h\}$, are defined as:

$$P\left(|q_{SS,1}| \geq T_{SS,1} \vee ... \vee |q_{SS,h}| \geq T_{SS,h} \mid H_0\right) P(H_0) \leq C_{REQ,0} \quad (19)$$

where $q_{SS,i}$ represents the corresponding SS test statistic. To avoid mixing up set and logical operators, this paper adopts the symbol $\vee$ for the logical operator "or" and $\wedge$ for the logical operator "and".

The continuity risk budget of SS detector is influenced by all fault modes, thus should account for multiple test statistic to ensure that the overall requirement is satisfied [29]. Precise assessment can be done towards the joint probability based on multidimensional probability density functions. To implement in real time, an upper bounding approach is employed:

$$P\left(|q_{SS,1}| \geq T_{SS,1} \vee ... \vee |q_{SS,h}| \geq T_{SS,h} \mid H_0\right) P(H_0) \leq \sum_{i=1}^{h} P\left(|q_{SS,i}| \geq T_{SS,i} \mid H_0\right) P(H_0) \quad (20)$$

Subsequently, the SS detection (normalized) threshold can be computed by:

$$\begin{aligned} T_{SS,i} &= \Phi^{-1}\left\{\frac{C_{REQ,i}}{2P(H_0)}\right\} \\ C_{REQ,0} &= \sum_{i=1}^{h} C_{REQ,i}, \text{ e.g., } C_{REQ,i} = \frac{C_{REQ,0}}{h} \end{aligned} \quad (21)$$

2) Loss of integrity: The integrity risk, or equivalently the probability of hazardous misleading information (HMI), is a joint probability defined as:

$$P_{HMI} = P(|\varepsilon_0| > l \wedge |q| < T) \quad (22)$$

with

- ε_0 the error of estimator
- l a specific alert limit that defines the hazardous situations
- q detection test statistic in RAIM/ARAIM approaches
- T detection threshold in RAIM/ARAIM approaches

which involves the event of *Hazardous Information* (HI) ($|\varepsilon_0| > l$), and the *No Detection* (ND) event ($|q| < T$).

When the multiple-hypothesis approach is employed, e.g., SS detector in ARAIM, the entire set of mutually exclusive, jointly exhaustive hypotheses should be accounted for to derive the overall probability of loss of integrity:

$$P_{HMI} = \sum_{i=0}^{h} P(|\varepsilon_0| > l \wedge |q_{SS,1}| < T_{SS,1} \wedge ... \wedge |q_{SS,h}| < T_{SS,h} \mid H_i) P(H_i) \quad (23)$$

A bound on the HMI probability can be established, e.g., [29]:

$$P_{HMI} \leq \sum_{i=0}^{h} P(|\varepsilon_i| + T_{SS,i}\sigma_{\Delta_i} > l \mid H_i) P(H_i) \leq I_{REQ} \quad (24)$$

with

- ε_i the error of estimator under each hypothesis H_i
- σ_{Δ_i} std of solution separations $\Delta_i = \varepsilon_i - \varepsilon_i$ for $i = 1, ..., h$

B. Framework of the set-based detector

1) Loss of continuity: The set-based detector takes the set-emptiness as the only criterion. Using the formulation of the solution set from Eq. 8, the expression for P_{FA} reads

$$P_{FA} = P\left(\mathcal{P} = \emptyset \mid H_0\right) \cdot P(H_0) \leq C_{REQ,0} \quad (25)$$

which is applicable in the definition of loss of continuity in Eq. 16 and Eq. 17.

The set-based detector differs from RB detector, as it performs on the state domain; and from SS detector, as it does not involve multiple test statistics but one single test criterion. It should be mentioned that the polytope $\mathcal{P}$ degenerates to an interval in the scalar state problem. In Sec. V, we present approaches for analytically determining the continuity risk for the set-based detection through an illustrative example.

2) Loss of integrity: Similar to the classical case, we can define the HMI probability in the interval case: We can formulate the *Protection* event when a set $\mathcal{B}$, e.g., interval in 1D, circle in 2D, and sphere in 3D, with the true position $\mathbf{x}^*$ as center and radius ℓ, encloses the polytope $\mathcal{P}$. In this case the maximum distance from the true position to any element of the feasible set solution, i.e. the polytope, is not larger than ℓ:

$$\mathcal{P} \subseteq \mathcal{B}(\mathbf{x}^*, \ell) \quad (26)$$

Figure 2 indicates the different situations in an two-dimensional conceptual sketch with three measurements: i) all elements of the feasible set solution ($\mathcal{P}$) has shorter or equal distance than ℓ to the true position. Hence, $\mathcal{P} \subseteq \mathcal{B}(\mathbf{x}^*, \ell)$; ii) the feasible set solution ($\mathcal{P}$) is only partially overlapped with $\mathcal{B}(\mathbf{x}^*, \ell)$, such that some elements of $\mathcal{P}$ has larger distance than ℓ to $\mathbf{x}^*$. This case belongs to $\mathcal{P} \nsubseteq \mathcal{B}(\mathbf{x}^*, \ell)$.

Subsequently, the probability of loss of integrity (P_{HMI}) is proposed to be expressed as:

$$P_{HMI} = P(\mathcal{P} \nsubseteq \mathcal{B}(\mathbf{x}^*, \ell) \wedge \mathcal{P} \neq \emptyset) \quad (27)$$

which is interpreted as the joint probability of

- *No Protection* ($\mathcal{P} \nsubseteq \mathcal{B}(\mathbf{x}^*, \ell)$): the feasible set solution $\mathcal{P}$ does not meet the alert limit for all elements, and
- *No Detection* ($\mathcal{P} \neq \emptyset$): the fault detection is not triggered, i.e., the measurements are considered self-consistent.

Considering the multiple hypothesis framework, the HMI probability is expressed as:

$$\begin{aligned} P_{HMI} &= \sum_{i=0}^{h} P(\mathcal{P} \nsubseteq \mathcal{B}(\mathbf{x}^*, \ell) \wedge \mathcal{P} \neq \emptyset \mid H_i) P(H_i) \\ &\leq I_{REQ} \end{aligned} \quad (28)$$

This formulation follows the structure of the classical one. However, it is noteworthy, that here the conditions rely only on the polytope.

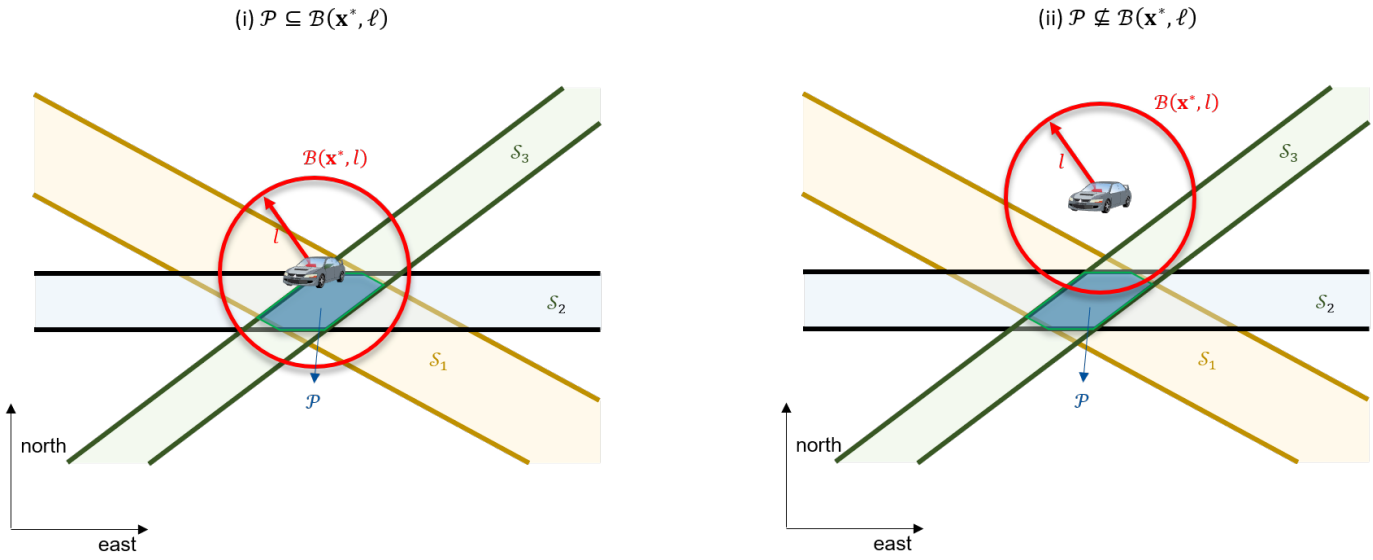

Fig. 2. Concept of *Protection* in case of intervals: i) the set solution polytope is protected ($\mathcal{P} \subseteq \mathcal{B}(\mathbf{x}^*, \ell)$); ii) the set solution polytope is not protected ($\mathcal{P} \nsubseteq \mathcal{B}(\mathbf{x}^*, \ell)$)

V. Detection Performance under Probabilistic Errors

To our knowledge, up until now, there is no study on the explicit evaluation for loss of continuity or loss of integrity. [22] gives a probabilistic interpretation of intervals and proposes a strategy of computing a lower bound of the probabilities for the computed set solution; Studies such as [14], [23], [30] apply this method in GNSS positioning to estimate high-integrity confidence zones. However, the risks are not yet characterized or verified with Monte Carlo simulations considering unknown distributed faults. We start this section with the example in Sec. V-A. Next, we discuss our evaluation approach in Sec. V-B, and then implement and validate with Monte Carlo simulations under a Gaussian error model in Sec. V-C.

A. A benchmark example

In this section, we consider a simulated scenario to demonstrate the detection procedure and the performance of the set-based detector in the probabilistic context. By setting prior probability requirements, we can assess the risk of loss of integrity and then perform a Monte Carlo simulation to observe the occurrence of those events for verification.

We directly take and adapt the canonical example from [31] to demonstrate without making unnecessarily complicated context. The problem is configured with three measurements solving a scalar estimation problem:

$$\mathbf{A}\mathbf{x} + \mathbf{f} \in \mathbf{y} - \mathbf{e} + [\mathbf{d}], \ \mathbf{A} = [1\ 1\ 1]^T \tag{29}$$

which degenerates to a mean estimator. For simplicity, we consider the case $\mathbf{e} \sim N(\mathbf{0}, \mathbf{I})$ and equal magnitude of the detector interval $[d_i] = [-d, d]$. The fault vector $\mathbf{f}$ represents three single-measurement faults, corresponding to three alternative hypotheses H_i, with unknown fault magnitude f_i:

$$\mathbf{f} = \begin{bmatrix} f_1 \\ 0 \\ 0 \end{bmatrix} \text{ or } \mathbf{f} = \begin{bmatrix} 0 \\ f_2 \\ 0 \end{bmatrix} \text{ or } \mathbf{f} = \begin{bmatrix} 0 \\ 0 \\ f_3 \end{bmatrix} \tag{30}$$

Integrity related parameters for evaluations are summarized in Tab. I, which is discussed in detail in the following subsections.

TABLE I
Integrity-related parameters for simulations.

Parameter	***Value***
Measurement error (σ)	$1\ m$
Continuity risk requirement C_{REQ}	10^{-6}
Prior probability of single-satellite fault P_f	10^{-3}
Prior probability of multiple-satellite fault	N/A
Prior probability for fault-free hypothesis $P(H_0)$	$1 - 3 \times 10^{-3}$
Integrity risk requirement I_{REQ}	N/A
Alert limit ℓ	variable

B. Risk evaluation

1) Probability of loss of continuity: Under H_0, the feasible set solution is obtained from the following inequality system based on Eq. 6:

$$\begin{cases} x \le y_1 + d, & -x \le -y_1 + d, \\ x \le y_2 + d, & -x \le -y_2 + d, \\ x \le y_3 + d, & -x \le -y_3 + d, \end{cases} \tag{31}$$

which results in the solution set:

$$\mathcal{P} := [\underline{x}, \overline{x}] = [\max(y_1, y_2, y_3) - d, \min(y_1, y_2, y_3) + d] \tag{32}$$

To achieve a non-empty solution set $\mathcal{P}$, we should have $\max(y_1, y_2, y_3) - \min(y_1, y_2, y_3) \le 2d$. A fault detection is triggered once the difference value excesses $2d$.

With n measurements $\mathbf{y} = [y_1, ..., y_n]^T$, the test statistic and criterion are expressed as:

$$W := \max(y_1, ..., y_n) - \min(y_1, ..., y_n) \leq 2d \tag{33}$$

which is a typical application of order statistics [32]:

Let $Y_1, Y_2, ..., Y_n$ be independent random variables drawn from a population with CDF $F(y)$ and PDF $f(y)$. Then the CDF of $Y_{(r:n)}$ (r-th order statistic, $r = 1, ..., n$) is given by:

$$\begin{aligned} F_{Y_{(r:n)}}(y) =& P(Y_{(r:n)} \leq y) \\ =& P(\textit{at least } r \textit{ of } Y_1, Y_2, ..., Y_n \textit{ are } \leq y) \\ =& \sum_{i=r}^{n} \binom{n}{i} F^i(y)[1 - F(y)]^{n-r} \end{aligned} \tag{34}$$

The binomial probability in the summand represents the probability that exactly r of the Y_i's are no greater than to y.

The test statistic W is in fact the difference of the n-th order statistic (maximum, $Y_{(n:n)}$) and the first order statistic (minimum, $Y_{(1:n)}$), i.e., sample range:

$$W = Y_{(n:n)} - Y_{(1:n)} \tag{35}$$

Its PDF reads

$$\begin{aligned} & f_W(w) \\ =& n(n-1) \int_{-\infty}^{\infty} f(y) \left[F(y+w) - F(y)\right]^{n-2} f(y+w) dy \end{aligned} \tag{36}$$

and CDF:

$$F_W(w) = n \int_{-\infty}^{\infty} f(y) \left[F(y+w) - F(y)\right]^{n-1} dy \tag{37}$$

Fig. 3 presents the CDF of W with varying Gaussian-distributed samples n. For the derivation of above equations,

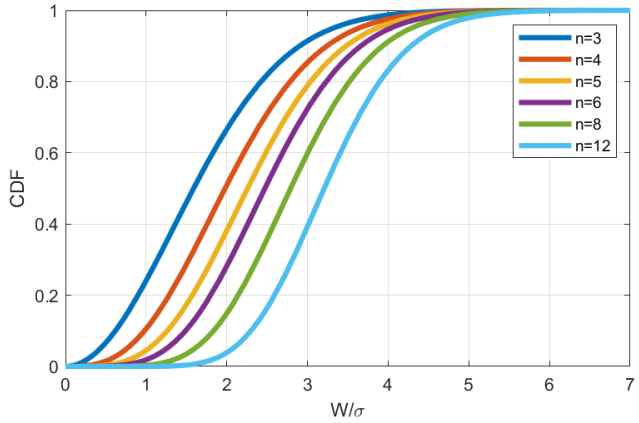

Fig. 3. CDF of test statistic $W := Y_{(n:n)} - Y_{(1:n)}$ with varying Gaussian-distributed samples n

readers of interest are referred to textbooks such as [32].

Subsequently, the probability of non-empty intersection, given $f(y)$ and $F(y)$, can be determined by:

$$\begin{aligned} & P(\text{non-empty intersection} \mid F(y), f(y) = F'(y)) \\ =& P(W \leq 2d \mid F(y), f(y) = F'(y)) \\ =& F_W(2d) \end{aligned} \tag{38}$$

Thus, the continuity risk can be assessed analytically through:

$$P\left(\mathcal{P} = \emptyset \mid H_0\right) = 1 - P(W \leq 2d \mid H_0) \tag{39}$$

If an arbitrary standard deviation σ is used for the observation, a normalisation by σ must be carried out in Eq. 32 which leads to the important *d-to-Sigma Ratio* ($\frac{d}{\sigma}$) that links the interval radius d with a Gaussian variance σ.

Subsequently, the interval radius d can be determined based on the continuity risk requirement, cf Eq. 25. For illustration, Fig. 4 displays the relations between $\frac{d}{\sigma}$, number of measurements n and detection probabilities under H_0. It depicts that the involvement of more measurements increases the probability of loss of continuity if the detector's interval radius is unchanged. While, given a fixed number of measurements, using wider intervals for detection tends to reduce the probability of loss of continuity.

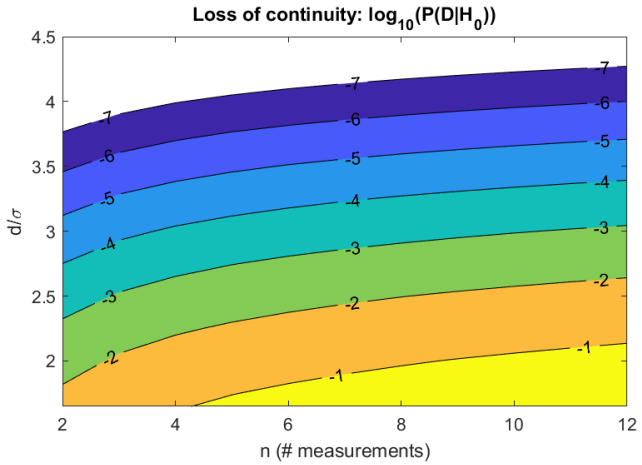

Fig. 4. Contour plot for the derived detection probabilities under H_0. The values are colored w.r.t varying $\frac{d}{\sigma}$ and number of measurements.

2) Probability of loss of integrity: The loss of integrity, discussed in Sec. IV, is a joint event of *No Protection* (NP) and *No Detection* (ND). Specifically, for the scalar estimation problem in the canonical example, we can express the set associated with alert limit as $\mathcal{B} = [x^* - \ell, x^* + \ell]$, and the feasible set solution $\mathcal{P}$:

- $\mathcal{P} = [\max\{\mathbf{y}\} - d, \min\{\mathbf{y}\} + d]$ under fault-free hypothesis H_0
- $\mathcal{P} = [\max\{\mathbf{y} + \mathbf{f}\} - d, \min\{\mathbf{y} + \mathbf{f}\} + d]$ under the hypothesis H_i, $i = 1, 2, 3$ with the unknown fault vector $\mathbf{f}$.

Therefore, the conditions of loss of integrity can be derived accordingly:

- H_0:
  - NP: $\max\{\mathbf{y}\} - \min\{\mathbf{y}\} \leq 2d$
  - ND: $\max\{\mathbf{y}\} \leq -\ell + d$ or $\min\{\mathbf{y}\} \geq \ell - d$
- H_i:
  - NP: $\max\{\mathbf{y} + \mathbf{f}\} - \min\{\mathbf{y} + \mathbf{f}\} \leq 2d$
  - ND: $\max\{\mathbf{y} + \mathbf{f}\} \leq -\ell + d$ or $\min\{\mathbf{y} + \mathbf{f}\} \geq \ell - d$

with $x^* = 0$, ℓ and $P(H_i)$ given as well as d determined from the continuity risk requirement in Eq. 39, the HMI probability can be evaluated with Eq. 28 using order statistics.

C. Experimental results

1) Loss of continuity: Based on the pre-defined continuity requirement $C_{REQ,0} = 10^{-6}$, we determine the interval for detection with radius $d = 3.608\sigma$. In a Monte Carlo simulation, we generate up to 10^7 random values for each measurement y_j, i.e., 10^7 epochs. Fig. 5 compares the simulation with evaluated probabilities and upper bounds for the detection events under H_0 with varying $\frac{d}{\sigma}$. The occurrence in Monte Carlo is very close to the analytical evaluated probability, and the detection criterion determined by order statistics method is verified.

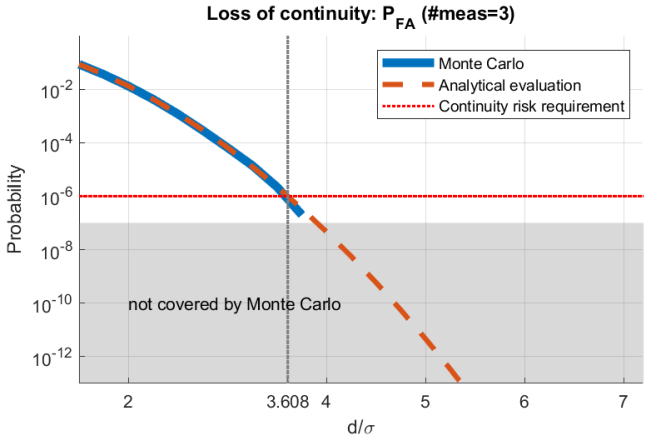

Fig. 5. Comparison of the analytically evaluation, Monte Carlo simulation for the detection probability under H_0. Values are computed for the illustrative example, varying with the $\frac{d}{\sigma}$. The Monte Carlo results are based on the same set of randomly generated measurements.

For the given continuity risk requirement, the detection threshold for RB and SS detectors can be determined for this canonical example, summarized in Tab. II. The continuity risk is equally allocated to each test statistic for SS detector as done in [29]. These thresholds are utilized in the next analysis.

TABLE II
DETECTION THRESHOLD FOR RB AND SS DETECTORS FROM PRE-DEFINED CONTINUITY RISK REQUIREMENT.

Detector	RB	SS
Threshold	5.256σ	5.103σ

2) Detectability: The set-based detector and classical RB/SS detectors are characterized by different parameters, and the set-based detector is not associated with a point estimator. Therefore, this section focuses on the detection "capability", or interpreted as the sensitivity to faults.

We perform the Monte Carlo simulation by adding a constant bias to the randomly generated measurements introduced in Sec. V-C1, and then observe the occurrence of the *Detection* events, i.e. $P(\mathrm{D}|\mathbf{f})$. By increasing the added bias magnitude, a comparison can be made in terms of the detection sensitivity to faults. The detection thresholds for RB and SS detectors and interval radius for set-based detector are introduced in Sec. V-C1. All three curves start at, or below 10^{-6} for the fault-free case.

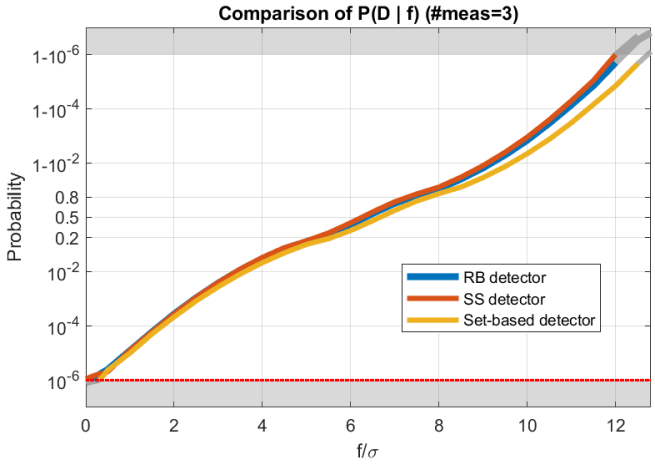

Fig. 6. Comparison of *Detection* probability $P(\mathrm{D} \mid \mathbf{f})$ in Monte Carlo simulation for RB, SS and set-based detector.

Fig. 6 compares the *Detection* probability $P(\mathrm{D} \mid \mathbf{f})$ for the RB, SS and set-based detector. The comparison result suggests that the SS detector outperforms RB detector slightly. A theoretical analysis in term of detection boundary in the parity space can be found in [29]. Meanwhile, the set-based detector performs relatively worse than the two classical detectors, particularly for greater biases. It may therefore be concluded that the classical RAIM/ARAIM detectors, especially the SS detector is optimal in terms of detection capability under Gaussian error assumption at this stage.

3) Loss of integrity: To understand the characteristics of integrity risk, we take again the randomly generated measurement dataset in Sec. V-C1 and perform multiple Monte Carlo runs: In the first run, we add a constant bias representing the fault to each of the three measurements with the pre-defined probability of single-measurement fault, cf Tab. I. The set-based detector, constructed by the detection intervals $[-d, d]$ in Sec. V-C1 which limits the false alert probability by given continuity risk requirement $C_{REQ,0} = 10^{-6}$, is then conducted over the obtained dataset including the faulty measurements. Subsequently, we can evaluate the probability of loss of integrity in Eq. 28 against various alert limits. In the following runs, the added bias is increased, whereas the other settings remain. The probability of loss of integrity is evaluated for all designed values of added bias and alert limit.

In Fig. 7, the probability of loss of integrity is colored with varying alert limit and added bias. A vertical section for $\ell = 4\sigma$ is plotted in Fig. 8 (i). The probability of *No Detection* ($P(\mathrm{ND} \mid \mathbf{f})$) is additionally plotted. It should be pointed out that $P(\mathrm{NP} \wedge \mathrm{ND} \mid \mathbf{f}) = P(\mathrm{NP} \mid \mathbf{f})$ because there is not separate estimator involved and P_{HMI} is evaluated over the same feasible set solution $\mathcal{P}$. Interestingly, the worst case

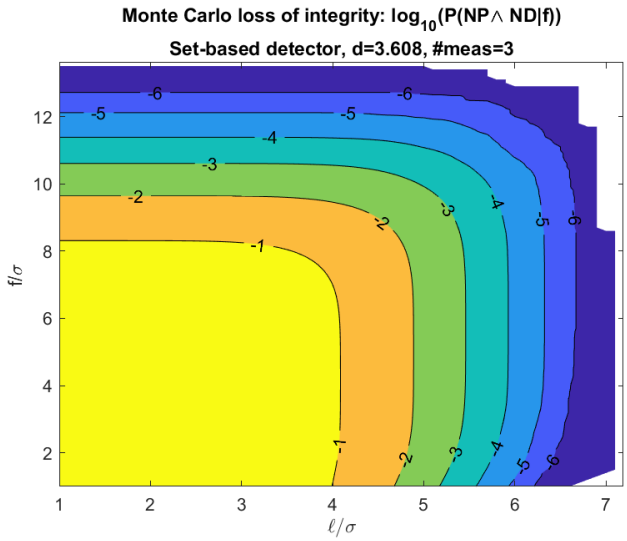

Fig. 7. Probability of loss of integrity for the set-based detector. The Monte Carlo results are based on the same set of randomly generated measurements with additional added single-measurement bias as fault f. The probabilities ($log_{10}(P(\text{NP} \wedge \text{ND} \mid \mathbf{f})$) are colored with varying alert limit ℓ/σ and fault magnitude ℓ/σ.

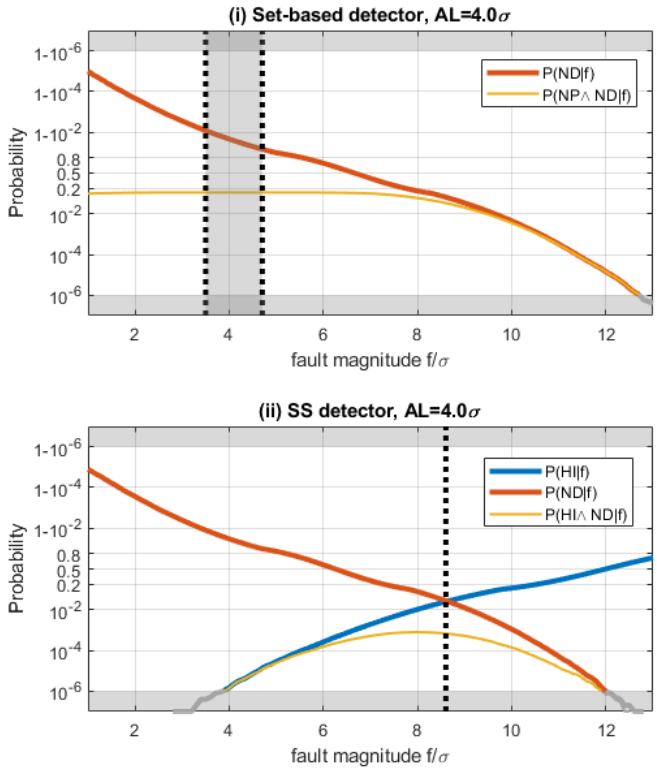

Fig. 8. Comparison of the worst case situation of loss of integrity between the set-based detector and SS detector against alert limit $\ell = 4\sigma$. The worst case situation for set-based detector is highlighted as the grey area, while that for SS detector is depicted as the black dashed line.

that maximizes the integrity risk indicates a "flat peak" as denoted by the grey range in Fig. 8 (i). This tendency can be found for all cases where $d \leq \ell$ from Fig. 7.

As a comparison, the probability of loss of integrity for SS detector against the same alert limit is plotted in Fig. 8 (ii). The worst case fault is obvious as it is recognized by the cross point of $P(\text{HI}|\mathbf{f})$ and $P(\text{ND}|\mathbf{f})$ curves, depicted as the black dashed line, whereas P_{HMI} is maximized. Furthermore, SS detector has greater worst case fault magnitude in this example. In this regard, the two detectors demonstrate completely different characteristics.

In Fig. 9, we compare the probability of loss of integrity directly for RB, SS and set-based detectors against various alert limits. A risk bound is calculated using the method in Eq. 24 cf [29] and plotted additionally as a black dashed curve. For this example, the difference between RB and SS detectors is insignificant. Meanwhile, the set-based detector presents a higher probability of loss of integrity, indicating conservative risk bounds. This can be understood in two aspects:

- The risk is evaluated over all elements of the feasible set solution, among which the less optimal estimates are weakening its performance.
- Different from the conventional RB and SS detectors, where a least squares estimator is assessed, the knowledge of Gaussian distribution is not fully taken advantage of for integrity in the set-based detector but only for continuity.

Therefore, a fair enough comparison still needs to be accomplished. In the sense of Gaussian error models, it is desired to optimize the set estimation for integrity purposes.

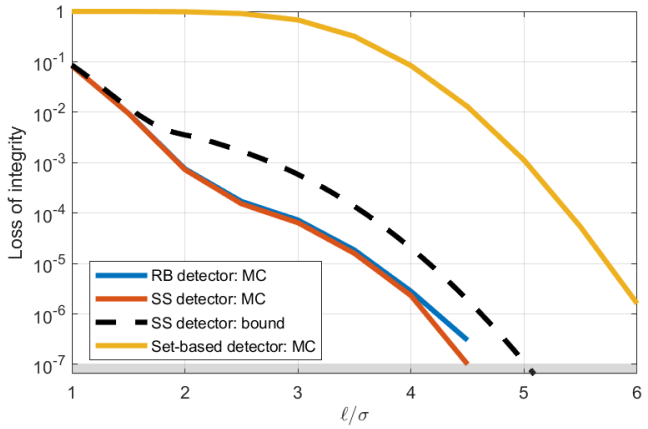

Fig. 9. Comparison of probability of loss of integrity for different detectors as the alert limit l varies. The Monte Carlo results are based on the same set of randomly generated measurements with additional added single-measurement bias as fault ($f = 8\sigma$). The detection thresholds are determined from continuity risk requirement. The black dashed curve presents IR bound for SS detector cf Eq. 24.

VI. Conclusions and Outlook

In this paper, we assess a set-based detector for GNSS integrity monitoring. The key contributions include: a) for-

mulating the fault detection for integrity monitoring in the context of measurement intervals; b) evaluating the probability of loss of continuity and loss of integrity for the set-based detector c) implementing and validating the detector in a benchmark example under the Gaussian assumption of measurement errors using Monte Carlo simulation, compared to classical RAIM/ARAIM detectors. The feasible set solution from simple measurement interval constraints assures high integrity of all point elements, however, at the price of relatively low availability in the sense of Gaussian assumptions. Therefore, the design of optimal set estimation for integrity is still needed for a better-performed set-based integrity monitor. In addition, future work should extend to multi-dimensional evaluation, and implementation in realistic GNSS satellite-user geometries.

REFERENCES

[1] RTCA SC-159, "Minimum operational performance standards (MOPS) for Global Positioning System/Satellite-Based Augmentation System airborne equipment," *RTCA/DO-229F*, 11 June 2006.

[2] M. Joerger, F.-C. Chan, S. Langel, and B. Pervan, "RAIM detector and estimator design to minimize the integrity risk," in *Proceedings of the 25th International Technical Meeting of the Satellite Division of the Institute of Navigation (ION GNSS 2012)*, 2012, pp. 2785–2807.

[3] J. Blanch, T. Walter, G. Berz, J. Burns, B. Clark, M. Joerger, M. Mabilleau, I. Martini, C. Milner, B. Pervan *et al.*, "Development of advanced RAIM minimum operational performance standards," in *Proceedings of the 32nd International Technical Meeting of the Satellite Division of The Institute of Navigation (ION GNSS+ 2019)*, Miami, Florida, September 2019, pp. 1381–1391.

[4] J. Blanch and T. Walter, "A fault detection and exclusion estimator designed for integrity," in *Proceedings of the 34th International Technical Meeting of the Satellite Division of The Institute of Navigation (ION GNSS+ 2021)*, 2021, pp. 1672–1686.

[5] J. Wendel, "GNSS pseudorange fault detection and exclusion with multiple outliers," in *Proceedings of the 35th International Technical Meeting of the Satellite Division of The Institute of Navigation (ION GNSS+ 2022)*, 2022, pp. 1481–1495.

[6] B. DeCleene, "Defining pseudorange integrity-overbounding," in *Proceedings of the 13th International Technical Meeting of the Satellite Division of The Institute of Navigation (ION GPS 2000)*, 2000, pp. 1916–1924.

[7] J. Rife, S. Pullen, B. Pervan, and P. Enge, "Paired overbounding and application to GPS augmentation," in *PLANS 2004. Position Location and Navigation Symposium (IEEE Cat. No. 04CH37556)*. IEEE, 2004, pp. 439–446.

[8] S. Schön, "Analyse und Optimierung geodätischer Messanordnungen unter besonderer Berücksichtigung des Intervallansatzes," *Dissertation. Deutsche Geodätische Kommission, DGK, Reihe C, Heft 567, München*, 2003.

[9] S. Schön and H. Kutterer, "Uncertainty in GPS networks due to remaining systematic errors: The interval approach," *Journal of Geodesy*, vol. 80, no. 3, pp. 150–162, 2006.

[10] J. Su and S. Schön, "Improved observation interval bounding for multi-GNSS integrity monitoring in urban navigation," in *Proceedings of the 34th International Technical Meeting of the Satellite Division of The Institute of Navigation (ION GNSS+ 2021)*, St. Louis, Missouri, September 2021, pp. 4141–4156.

[11] ——, "Bounding the residual tropospheric error by interval analysis," in *International Association of Geodesy Symposia*. Berlin, Heidelberg: Springer Berlin Heidelberg, 2022, pp. 1–10.

[12] R. E. Moore, R. B. Kearfott, and M. J. Cloud, *Introduction to interval analysis*. SIAM, 2009.

[13] D. Meizel, O. Lévêque, L. Jaulin, and E. Walter, "Initial localization by set inversion," *IEEE transactions on robotics and Automation*, vol. 18, no. 6, pp. 966–971, 2002.

[14] V. Drevelle and P. Bonnifait, "High integrity GNSS location zone characterization using interval analysis," in *Proceedings of the 22nd International Technical Meeting of the Satellite Division of The Institute of Navigation (ION GNSS 2009)*, 2009, pp. 2178–2187.

[15] S. Schön and H. Kutterer, "Using zonotopes for overestimation-free interval least-squares–some geodetic applications," *Reliable Computing*, vol. 11, no. 2, pp. 137–155, 2005.

[16] J. Su and S. Schön, "Deterministic approaches for bounding GNSS uncertainty: A comparative analysis," in *2022 10th ESA Workshop on Satellite Navigation Technologies and European Workshop on GNSS Signals and Signal Processing (NAVITEC)*, Noordwijk, The Netherlands, April 2022, pp. 1–8.

[17] H. Dbouk and S. Schön, "Reliable bounding zones and inconsistency measures for GPS positioning using geometrical constraints," *Acta Cybernetica*, vol. 24, no. 3, pp. 573–591, 2020.

[18] J. Su and S. Schön, "Advances in deterministic approaches for bounding uncertainty and integrity monitoring of autonomous navigation," in *Proceedings of the 35th International Technical Meeting of the Satellite Division of The Institute of Navigation (ION GNSS+ 2022)*, Denver, Colorado, September 2022, pp. 1442–1454.

[19] M. Kieffer, L. Jaulin, É. Walter, and D. Meizel, "Robust autonomous robot localization using interval analysis," *Reliable computing*, vol. 6, no. 3, pp. 337–362, 2000.

[20] F. Le Bars, R. Sanchez, L. Jaulin, S. Rohou, and A. Rauh, "An online interval-based inertial navigation system for control purposes of autonomous boats," *Frontiers in Control Engineering*, vol. 2, p. 22, 2022.

[21] S. Ifqir, C. Combastel, and A. Zolghadri, "Set-based multi-sensor data fusion for integrated navigation systems," in *2021 5th International Conference on Control and Fault-Tolerant Systems (SysTol)*. IEEE, 2021, pp. 219–224.

[22] L. Jaulin, "Set-membership localization with probabilistic errors," *Robotics and Autonomous Systems*, vol. 59, no. 6, pp. 489–495, 2011.

[23] L. C. Bento, P. Bonnifait, and U. J. Nunes, "Cooperative GNSS positioning aided by road-features measurements," *Transportation Research Part C: Emerging Technologies*, vol. 79, pp. 42–57, 2017.

[24] L. Jaulin, M. Kieffer, O. Didrit, and E. Walter, *Applied interval analysis: With examples in parameter and state estimation, robust control and robotics*. London: Springer, 2001.

[25] G. M. Ziegler, *Lectures on polytopes*, ser. Graduate texts in mathematics. New York: Springer, 1995, vol. 152.

[26] D. Eppstein, "Zonohedra and zonotopes," Dept. of Information & Computer Science U.C. Irvine, CA, 92717, Tech. Rep., 1995. [Online]. Available: http://www.ics.uci.edu/˜eppstein

[27] ICAO, "Annex 10 to the convention on civil aviation-aeronautical communications," vol. 1 (Radio Navigation Aids), 2018.

[28] Y. Zhai, M. Joerger, and B. Pervan, "Continuity and availability in dual-frequency multi-constellation ARAIM," in *Proceedings of the 28th International Technical Meeting of the Satellite Division of The Institute of Navigation (ION GNSS+ 2015)*, 2015, pp. 664–674.

[29] M. Joerger and B. Pervan, "Solution separation and chi-squared ARAIM for fault detection and exclusion," in *2014 IEEE/ION Position, Location and Navigation Symposium-PLANS 2014*. IEEE, 2014, pp. 294–307.

[30] V. Drevelle and P. Bonnifait, "Reliable positioning domain computation for urban navigation," *IEEE Intelligent Transportation Systems Magazine*, vol. 5, no. 3, pp. 21–29, 2013.

[31] M. Joerger, S. Stevanovic, F.-C. Chan, S. Langel, and B. Pervan, "Integrity risk and continuity risk for fault detection and exclusion using solution separation ARAIM," in *Proceedings of the 26th International Technical Meeting of the Satellite Division of The Institute of Navigation (ION GNSS+ 2013)*, 2013, pp. 2702–2722.

[32] H. A. David and H. N. Nagaraja, *Order statistics*. John Wiley & Sons, 2004.